No-Reference Quality Assessment of Underwater Image Enhancement*

Xiao Yi[a], Qiuping Jiang[a,*], Wei Zhou[b]

[a]School of Information Science and Engineering, Ningbo University, Ningbo 315211, China.
[b]School of Computer Science and Informatics, Cardiff University, Cardiff CF10 3AT, United Kingdom.

Abstract

Due to the attenuation and scattering of light in the water medium, real-world underwater images usually suffer from diverse quality defects, such as color casts, low contrast, and reduced visibility, etc. These quality defects accordingly cause adverse effects on underwater images in practical applications. To tackle the problem, many underwater image enhancement (UIE) techniques have been proposed for improving the quality of raw underwater images, showing heterogeneous performances regarding the enhanced results. Therefore, designing an objective quality metric that can effectively predict the visual quality of enhanced underwater images is desirable. In this paper, we propose a highly efficient yet accurate no-reference quality assessment method to evaluate different UIE results by analyzing the statistics of underwater images. Specifically, we first extract quality-aware features in terms of three key aspects: 1) colorfulness; 2) contrast; 3) visibility. Then, a quality regression model is trained to map the extracted features to subjective scores for enhanced underwater images. Given a testing underwater image, we also first extract its corresponding quality-aware feature vector and feed it into the trained quality regression model for quality prediction. We conduct extensive experiments on two databases to demonstrate the superiority of our proposed approach. The code is available at https://github.com/yia-yuese/NR-UIQA.

Keywords: Underwater image enhancement, Image quality assessment, No-reference

1. Introduction

The exploitation and utilization of marine resources play an essential role in maritime economic development. As an important way to record visual information of underwater scenes, high-quality underwater optical imaging plays a vital role in the marine industry [1, 2, 3, 4, 5, 6, 7]. However, it is quite challenging due to the complicated and volatile underwater environment. As a consequence, the visual quality of raw underwater images is often prone to different kinds of degradations, such as color casts, reduced contrast, and poor visibility, etc. Therefore, many underwater image enhancement (UIE) algorithms have been developed to improve the visual quality of underwater images in the literature [8, 9, 10, 11, 12, 13, 14, 15, 16, 17, 18, 19, 20, 21, 22, 23, 24, 25, 26]. Despite this, objective metrics that can fairly and effectively evaluate the enhanced results of different UIE algorithms remain less investigated.

Intuitively, image quality assessment (IQA) is based on human visual perception and therefore subjective evaluation is considered to be the most reliable way. However, subjective evaluation is criticized for being cumbersome and time-consuming. A more practical way to evaluate image quality is to develop an accurate and automatic objective metric that can predict quality highly correlated with the results from human judgment. In general, objective IQA methods can be divided into three categories [27], including full reference (FR), reduced reference (RR), and no reference (NR). The FR IQA methods

*This is an example for title footnote coding.
*Corresponding author:
Email address: jiangqiuping@nbu.edu.cn (Qiuping Jiang)

utilize full information of the corresponding distortion-free counterpart as a reference for quality evaluation [28, 29, 30]. The RR IQA methods depend on partial information from the distortion-free image for quality evaluation [31, 32]. The NR IQA methods only rely on the distorted image for quality prediction [33, 34, 35, 36, 37, 38, 39, 40, 41, 42, 43, 44, 45, 46, 47, 48, 49]. As for the underwater scenario, it is impractical to obtain the original underwater image in real-world underwater environments as reference, the NR pipeline becomes the most suitable way in real applications.

Currently, the field of underwater image quality assessment is experiencing an actively evolving and vibrant phase, yielding a multitude of significant research outcomes. Yang et al. [50] introduced the Underwater Color Image Quality Evaluation (UCIQE) metric based on a linear combination of chromaticity standard deviation, luminance contrast, and average saturation.Panetta et al.[51] overcame the limitation of UCIQE and proposed an underwater image quality method (UIQM) by considering color, sharpness, and contrast. Wang et al. [52] proposed the CCF metric for underwater image quality assessment, encompassing components such as chromaticity measurement, contrast measurement, and fog density measurement. Recently, Yang et al.[53] proposed an image quality evaluation metric called FDUM that combines color, contrast, and sharpness clues. FDUM considers the degradation effects of underwater images and the different sensitivities of the human visual system to high-frequency and low-frequency information of images. Lin et al. [54] employed a simulated contrast method for the evaluation of enhanced underwater images, while Zheng et al. [55] introduced the Underwater Image Fidelity (UIF) metric, which is rooted in naturalness, sharpness, and structural indicators within the CIELab color space. Additionally, Guo [56] introduced a novel objective image quality metric called UWEQM which considers the physical characteristics of the underwater environment and relevant attributes of the human visual system. Jiang et al. [57] proposed an effective method for evaluating the quality of enhanced underwater images (NUIQ), which transforms RGB underwater images into the opponent color (OC) space and extract color, luminance, and structural features in this space to achieve objective quality assessment. Furthermore, there are also several other research endeavors [58, 59, 60] also dedicated to the quality assessment of enhanced underwater images. Overall, these research endeavors constitute a rich and diverse landscape within the field of underwater image quality assessment.

However, these methods still suffer from certain limitations. In the methods such as UCIQE [50], UIQM [51], CCF [52], and FDUM [53], manually defined weights ars applied to combine the extracted feature attributes, resulting in suboptimal performance and limited generalization capabilities. Lin et al.'s work [54] relies on subjective methods for quality assessment research, which are impractical for large-scale dataset investigations and cannot be applied effectively in practical applications. In the work of Guo et al. [58], the authors only conducted experiments on a self-constructed small-scale dataset, comprising only 200 underwater enhanced images, which may constrain its performance on larger datasets. Additionally, the used feature extraction methodology entirely relies on [51]. In comparison to UIF [55], UWEQM [56], NUIQ [57], UIQI [59], and GLCQE [60], although they exhibit superior performance in addressing certain drawbacks of previous methodologies and pay more significant attention to issues like color distortion, insufficient luminance, and detail blurring in underwater images, they do not adequately incorporate prior statistical data from high-quality underwater images as reference for the assessment of degraded underwater image quality. Therefore, there is a need for further exploration to enhance the accuracy and robustness of underwater image quality assessment metrics.

Inspired by the aforementioned underwater image quality assessment metrics, we in this paper propose a novel NR-IQA method for evaluating the quality of enhanced underwater images. It is known that, in subjective experiments, human observers rate underwater image image quality mainly according to the perception of colorfulness, contrast, and visibility. Therefore, our proposed method focuses on exploiting three types of statistics respectively corresponding to colorfulness, contrast, and visibility of enhanced underwater images. In addition, the RGB channel pixels of underwater images conform to the particular prior of Rayleigh distribution [61] is taken into consideration. To summarize, this paper makes the following contributions:

1) Based on the degradation characteristics of underwater images, we propose a novel NR-IQA method for evaluating the quality of enhanced underwater images,

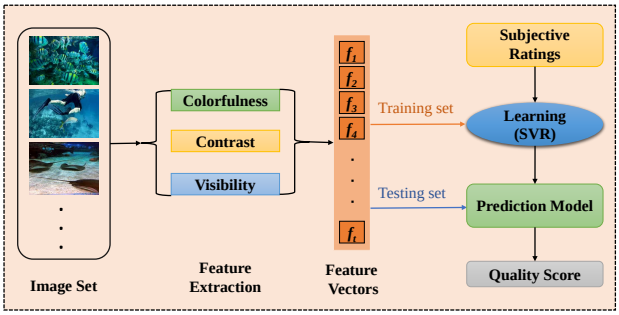

Figure 1: Pipeline of the proposed NR IQA method.

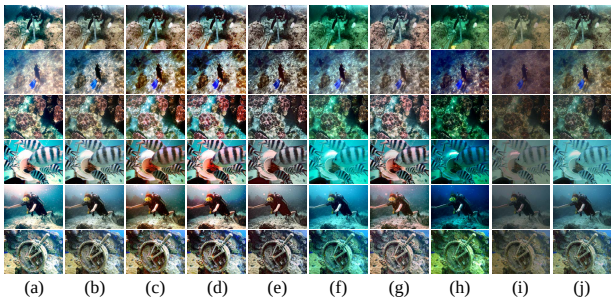

Figure 2: Image examples generated by different UIE algorithms in the SAUD database. (a) BL-TM [13], (b) HP-based [14], (c) RD-based[15], (d) Retinex [16], (e) RGHS [17], (f) TS-based [18], (g) UDCP [20], (h) UWCNN [21], (i) GL-Net [22], (j) Water-Net [23]

which comprehensively exploits the statistics of colorfulness, contrast, and visibility.

2) By combining with the prior knowledge that underwater images conform to Rayleigh distribution, the image quantification color feature is designed.

3) Given the importance of contrast for underwater images after enhancement, we propose a new method to estimate the contrast by computing the entropy difference and moment statistics. Experiments show that our method is more consistent with subjective scores compared to state-of-the-art quality assessment models.

The rest of this paper is divided into three sections. In Section II, we introduce our proposed NR quality assessment method for underwater enhancement in detail. Section III then shows the experimental results and analysis. Finally, we conclude the paper in Section IV.

2. Proposed Method

We illustrate the framework of our proposed method in Fig. 1. For each enhanced underwater image, we first extract three sets of quality-aware features related to color, contrast, and visibility, respectively, and then combine them into a feature vector. After that, the support vector regression (SVR) model is learned to map the extracted feature vectors into the corresponding subjective quality scores. Finally, the quality of the test image can be predicted by the learned SVR model.

2.1. Image Colorfulness

The underwater images easily suffer from visual problems regarding color casts. Here, we provide some image examples generated by various UIE algorithms, as shown in Fig. 2. We can see that the abilities of those UIE algorithms to correct color casts are different. Moreover, the higher the underwater image quality, the more color details, and fewer color casts. Therefore, color is a vital image attribute in underwater visual environments, which is vital for measuring enhanced underwater image quality. Considering that saturation or color purity can reflect color richness than image brightness, we first extract the global mean for the test image in the saturation channel to represent its color intensity

$$\mathrm{C}_{s1} = \frac{1}{N}\sum_{x,y} S(x,y), \tag{1}$$

where N represents the total pixel number. $S(x,y)$ is the image in the converted saturation channel.

Second, the research in human vision reveals that color perception is generally carried out in the opposing color spaces. Therefore, we then convert the image to the opponent color space [62] to estimate the color information by calculating the contrast energy C_f of the three opponent color components[63] by

$$C_f = \frac{\alpha\xi(I_f)}{\xi(I_f)+\alpha\tau} - \theta_f, \quad f \in \{R_1, R_2, R_3\}, \tag{2}$$

where R_1, R_2, and R_3 denote the red-green, yellow-blue and gray channels, respectively. Among them, $R_1 = R - G, R_2 = (R+G)/2 - B$, $R_3 = 0.299 * \mathrm{R} + 0.587 * \mathrm{G} + 0.114 * \mathrm{B}$, $\xi(I_f) =$

(a) (b) (c)

Figure 3: The MOS values of (a), (b), (c) are 79, 52, and 14, respectively.

$\sqrt{(I_f \otimes {h_v}^2 + I_f \otimes {h_h}^2}$, and $\otimes$ indicates the convolution operation. h_v and h_h are the vertical as well as horizontal second derivatives for the Gaussian functions. In addition, τ is the contrast gain that is applied to correct and divide filter responses to explain the nonlinear contrast gain control process of the human visual cortex. α and $theta_f$ are the maximum value of and the threshold to constrain noise. The settings of all these parameters can be found in [28]. After that, the mean values of the contrast energy are extracted as $C_{s2} = \{C_{R1}, C_{R2}, C_{R3}, \}$.

Third, it is possible to convert images from the original RGB space to the LMS space of a cone. We then calculate the contrast energy in both blue-yellow and luminance channels. This is widely used in the task of color constancy[62, 64, 65]. The color can be expressed as the integration of variance and mean[66]

$$C_{s3} = 0.3\sqrt{\mu_{R_1}^2 + \mu_{R_2}^2} + \sqrt{\sigma_{R_1}^2 + \sigma_{R_2}^2}, \tag{3}$$

where $\sigma_{R_1}^2$, $\sigma_{R_1}^2$, $\mu_{R_1}^2$ and $\mu_{R_2}^2$ represent the variance and average of image pixels in red-green and yellow-blue color spaces. Here, the mean of C_{s3} can be used as an additional colorfulness feature.

In Fig. 3, we show several enhanced underwater images with the corresponding subjective quality scores. The colorfulness features obtained from equations (1), (2), and (3) above are (a) {0.48, 4.94, 4.05, 4.37, 27.84}, (b) {0.37, 1.72, 1.62, 2.78, 19.17}, (c) {0.27, 1.65, 1.28, 1.58, 9.12}. As can be seen in the figure, with the decrease in subjective quality, the colorfulness feature values also reduce, showing that these features are good indicators to evaluate underwater image quality in terms of the color attribute.

In order to measure image quality in pixel space, various image-level statistics are exploited based on fitting a probability density function (PDF) [67]. For example, the mean, standard deviation, skewness, kurtosis, and entropy usually serve as image-level statistical priors. Previous studies show that the Rayleigh distribution is one of the best distributions for the intensity histogram of underwater images[61, 68]. Therefore, we utilize the PDF of Rayleigh distribution as

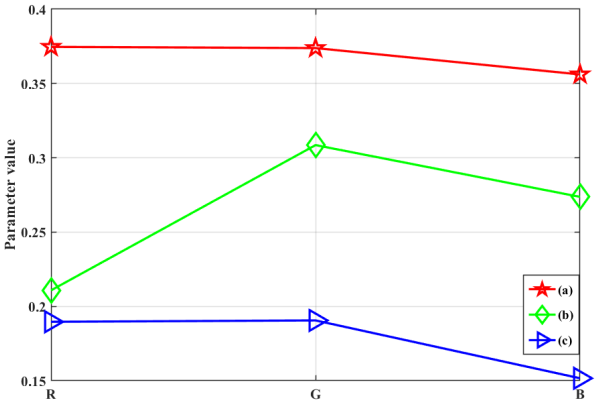

Figure 4: The fitted Rayleigh distribution shape parameters of the RGB channel histogram of the example images (a), (b), (c) in Fig. 3.

$$f(x) = \frac{x}{\sigma^2}\exp(-\frac{x^2}{2\sigma^2}), \quad x > 0, \tag{4}$$

where σ is the shape parameter of Rayleigh distribution. We then take the shape parameters of RGB channels for enhanced underwater images as complementary colorfulness features.

Taken images in Fig. 3 as examples, the shape parameter values of Rayleigh distribution for RGB channels are shown in Fig. 4 We can observe that the higher the image quality, the higher the shape parameters. Therefore, the underwater image quality and the shape parameters of Rayleigh distribution for RGB channels have certain regularity. In other words, these parameters can be used to represent colorfulness and are denoted as $R_1 = \{\sigma_R, \sigma_G, \sigma_B\}$.

Additionally, to capture the difference in the distribution of the RGB channel histogram fitting curves of distorted and high-quality underwater images, we employ the well-known K-L divergence to measure the distance between the two distributions. Specifically, assuming that m and n are the histogram distributions of distorted and high-quality underwater images, respectively. The K-L

(a) (b) (c)

Figure 5: The MOS values of (a-c) are 79, 44, and 26, respectively.

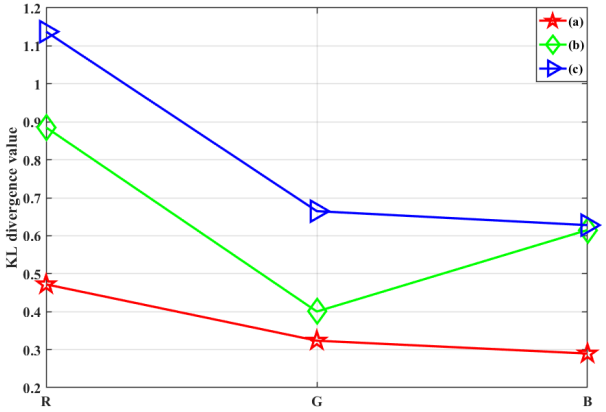

Figure 6: K-L divergence values of the Rayleigh distribution curve for the high-quality underwater images and the example images in Fig. 5.

divergence between m and n is defined by

$$D_{KL}(m||n) = -\int m(x)\log n(x)dx + \int m(x)\log m(x)dx. \tag{5}$$

We use Fig. 5 as the underwater images for testing. Fig. 6 shows the K-L divergence of the Rayleigh distribution between the distorted and high-quality underwater images. If the distribution of the test underwater image is closer to that of the high-quality underwater image, we have a smaller K-L divergence, indicating that the quality of the test image is better, and vice versa. It should also be noted that the distribution of high-quality images is from [61]. Here, we denote the K-L divergence features for colorfulness as $D = \{D_R, D_G, D_B\}$.

2.2. Image Contrast

Contrast is an essential property of images and is highly related to the quality of the image. Information entropy is a global measure that characterizes the average amount

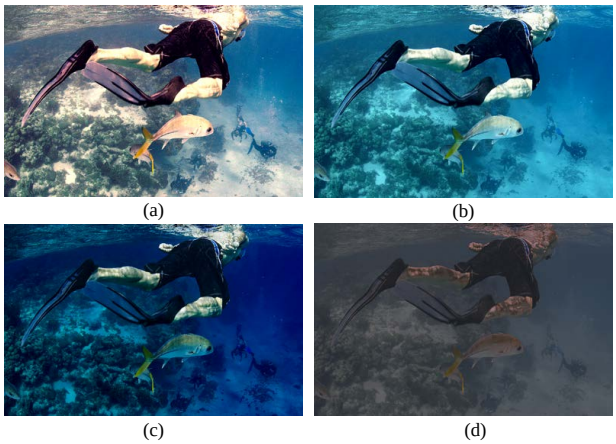

(a) (b) (c) (d)

Figure 7: The MOS values of (a-d) are 69, 62, 19, and 8 respectively.

of information in an image, which is commonly used to reflect image contrast. Generally, greater entropy means that the image has more excellent contrast and, thus, better visual quality. As shown in Fig. 7, (a) is an image with good quality, and figures (b-d) are under slight, extensive, and severe underexposure, respectively. We can observe more details in (a) with relatively high contrast, while largely reduced details in (d) due to the low contrast leading to the worst quality. Motivated by these observations, we extract contrast-related features for evaluating underwater enhancement.

We notice that lower contrast can cause more pixel intensities to move towards the minimum value (i.e., 0). That is, when the pixel deviation is more significant, the degree of contrast deficiency increases. Too bright or too dark would affect the image contrast. To measure this effect, we first create intermediate images $I_{m_k}, k \in \{1, 2, ..., K\}$. After adding the ΔI_{m_i} value to the gray-scale image I, the intermediate images I_{m_k} are obtained by

$$I_{m_k} = I + \Delta I_{m_k}, \tag{6}$$

where $\Delta I_{m_k} = \{\pm 120, \pm 90, \pm 60, \pm 30\}$, K denotes the value of the k-th ΔI_{m_k}, If I_{m_k} value is above 255 and below 0, we set it set to 255 and 0, respectively. With these intermediate images, we calculate their information entropy as

$$E(p) = -\sum_n p_n \cdot \log p_n, \tag{7}$$

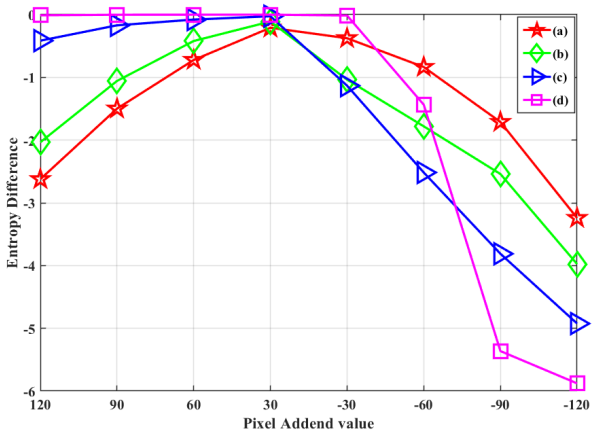

Figure 8: The entropy difference E_{d_i} changes with the respect to ΔI_{m_i}, where the corresponding curves of Fig. 7 (a-d) are illustrated in red, green, blue, and purple.

where p_n represents the probability density. Then, the contrast can be revealed by the entropy difference, which is computed between image I and the resulting intermediate image I_{m_k}. The operation is formulated as

$$E_{d_k} = E_{I_{m_k}} - E_I, \tag{8}$$

where E_I and $E_{I_{m_k}}$ are the entropies of image I and the generated intermediate image I_{m_k}, respectively.

Fig. 8 shows that E_{d_i} changes along with the image pixel intensity. This may be because when the image is processed with the value of ΔI_{m_i}, the pixel probability near the end of the dynamic range increases, which causes a decrease in entropy. That is, a larger probability transformation results in a larger entropy difference. For a test image with good quality (e.g., Fig. 7(a)), its entropy difference curve is approximately symmetric because the pixel values are clustered in the middle position of the dynamic range [69]. And the pixels at both ends deliver similar probability changes regarding the symmetric addend, and the entropy difference curve approximates a symmetric distribution. In contrast, the entropy difference curve of a low-contrast image becomes asymmetrical. This is due to the uneven distribution of pixels in the low-contrast image, and its pixel value is either higher or lower.

Except for the global contrast measure of enhanced underwater images, we employ the local contrast feature extraction [70] Specifically, we divide the image into patches with the resolution of 8×8 and then calculate the entropy difference as the global operation. After that, the average E_{ldi} of the entropy difference for each image patch is computed to measure the local contrast of the test image. In addition, to compensate for the abnormal distribution of image pixels, we also extract the moment statistic $M = \{M_\partial, M_\delta, M_s, M_k\}$ to estimate the image contrast. These indlude the first-order mean $M_\partial = \gamma(I)$, second-order standard deviation $M_\delta = \sqrt{\gamma[I - \gamma(I)^2]}$, third-order slice skewness $M_s = \frac{\gamma[I-\gamma(I)^3]}{(M_\delta)^3}$, and fourth-order kurtosis $M_k = \frac{\gamma[I-\gamma(I)^4]}{(M_\delta)^4} - 3$. And $\gamma(.)$ represents the averaging operator.

2.3. Image Visibility

Due to the complex imaging environment of underwater images, underwater images are inevitably affected by wavelength-dependent absorption, and scattering [67, 71, 68, 72]. Therefore, the visibility of underwater images is an essential attribute in evaluating quality. When the image visibility is high, it indicates that the quality is relatively good, and vice versa.

In general, we can measure the image structures or edges to assess the image visibility [73, 74, 75]. Here, we use the logarithmic energy of each high-frequency subband obtained by the wavelet transform of the test image. To be specific, a three-level decomposition of Cohen-Daubechies-Fauraue 9/7 filters [76] is applied to decompose the image into multiple subbands. An example is shown in Fig. 9. For mathematical formula, we use $E_{LH,l}$, $E_{HL,l}$ and $E_{HH,l}$ to denote the logarithmic energy of the discrete wavelet transform LH, HL, and HH subbands:

$$\begin{cases} E_{LH,l} = \log_{10}[1 + \frac{1}{K_l}\sum_i LH_l^2(i)] \\ E_{HL,l} = \log_{10}[1 + \frac{1}{K_l}\sum_i HL_l^2(i)] \\ E_{HH,l} = \log_{10}[1 + \frac{1}{K_l}\sum_i HH_l^2(i)] \end{cases} \tag{9}$$

Where i denotes the pixel index of the image and K_l is the number of subband coefficients for decomposition level l.

$$E_l = (1 - \alpha) \cdot \frac{E_{LH,l} + E_{HL,l}}{2} + \alpha \cdot E_{HH,l}, \tag{10}$$

where parameter α is the weight given to the decomposed HH subband. Here, we set $\alpha = 0.8$. Fig. 11

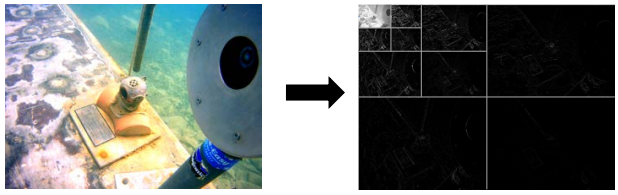

Figure 9: Schematic diagram of three-level wavelet transform of an underwater image.

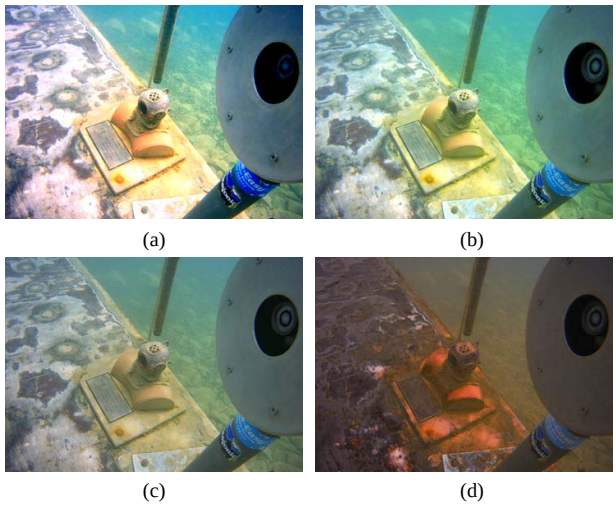

Figure 10: (a)-(d) The mass fractions are represented by MOS values, which are 63, 52, 45, and 2, respectively.

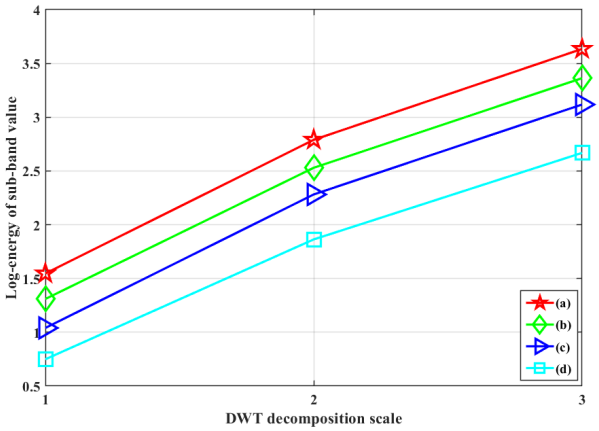

Figure 11: Subband energy distribution of the example images of Fig. 10(a)-(d).

Table 1: Summary of The Extracted 42-Dimensional Features.

Index	Eeature Typy	Symbol	Feature Description	Feature ID
1	Image colorfulness	C_{s1},C_{R1},C_{R2}, C_{R3},C_{s3},R,D	Evaluation of image colorfulness	$f_{01} - f_{11}$
2	Image exposure	E_{d_i},E_{ldi},M	Measurement of image exposure	$f_{12} - f_{39}$
3	Image naturalness	E_1,E_2,E_3	Assessment of mage naturalness	$f_{40} - f_{42}$

shows the high-frequency subband energies of the three-level wavelet transform for the test images in Fig. 10 (a)-(d). It can be found that as the underwater image quality decreases, the logarithmic energy decreases, and it increases as the decomposition scale becomes more extensive. Therefore, the wavelet subband energy can be used to evaluate image visibility.

2.4. Quality Regression

With the above processes, we have extracted three kinds of features by considering three image attributes of underwater images, i.e., color, contrast, and visibility, which are closely relevant with the quality of underwater images. Overall, we extract 42-dimensional features in total. For a better understanding, we have summarized these features in Table 1.

Based on the extracted quality attributes of colorfulness, contrast, and visibility from enhanced underwater images, we resort to the well-known support vector regression (SVR) model [77] for mapping the features onto image quality. The standard formula of SVR is

$$\begin{aligned} \min_{w,B,\tau,\hat{\tau}} \ & \tfrac{1}{2}\|w\|_2^2 + C\sum_{z=1}^{Z}(\tau_z + \hat{\tau}_z) \\ s.t. \ & w^T\phi(x_z) + B - y_z \le \varepsilon + \tau_z \\ & y_z - w^T\phi(x_z) - B \le \varepsilon + \hat{\tau}_z \\ & \tau, \hat{\tau} \ge 0, z = 1, 2, ...Z \end{aligned} \tag{11}$$

where B represents the bias parameter. $\varepsilon > 0$ and $C > 0$. Moreover, τ and $\hat{\tau}$ indicate slack variables. x_z and y_z denote the concatenated feature vector and subjective quality, respectively. $K(x_z, x_j) = \phi(x_z)^T\phi(x_j)$ is the nonlinear kernel function. In our experiments, we employ the radial

basis function kernel. According to the training sample $D = \{(x_1, y_1), (x_2, y_2), ..., (x_z, y_z)\}$, the parameter ($\varepsilon$, C, ρ) can be obtained by minimizing the error value between the predictions and ground truth. After computing these parameters, a predictive model can be built. Then, the quality of a given test image can be obtained by inputting the 42-dimensional image features into the trained SVR model.

3. Experimental Results and Analysis

3.1. Protocols

In the experiments, we compare the proposed method with state-of-the-art quality assessment methods. Specifically, we select 15 existing mainstream NR quality metrics, consisting of 10 general NR IQA metrics (i.e., DIIVINE [33], BIQME [39], BLIINDS-II [40], BRISQUE [41], FRIQUEE [42], GM-LOG [44], GWH-GLBP [45], NFERM [46], NRSL [47], PCRL [48]) and the metrics specifically designed for evaluating underwater image quality (i.e., UCIQE [50], UIQM [51], CCF [52], FDUM [53], NUIQ [57]).

In addition, these metrics can be categorized into two different types: learning-based and non-learning based. The learning-based methods include DIIVINE [33], BIQME [39], BLIINDS-II [40], BRISQUE [41], FRIQUEE [42], GM-LOG [44], GWH-GLBP [45], NFERM [46], NRSL [47], PCRL [48], NUIQ [57], while the non-learning-based methods include UCIQE [50], UIQM [51], CCF [52], FDUM [53]. All the compared NR quality assessment algorithms are implemented from the public codes. For learning-based methods, we follow the same testing principles as the proposed method and optimize the learned network parameters for the best performance.

We split the database into 80% and 20% for training and testing, respectively. The training-testing random split process is carried out 1,000 times to prevent performance bias. Four evaluation criteria are used, including Spearman's rank correlation coefficient (SRCC), Kendall rank correlation coefficient (KRCC), Pearson correlation coefficient (PLCC), and Root-mean-square error (RMSE). Finally, the mean values of these criteria are calculated as the final performance results are calculated as the final performance for each method in 1,000 tests. For non-learning-based methods, the results are obtained by computing the SRCC, KRCC, PLCC, and RMSE between estimated scores and their corresponding subjective scores (i.e., MOS) for all images in the database.

Table 2: Performance Comparison of Different NR-IQA on The SAUD Dataset and The UID2021 Dataset.

Metrics	SAUD [57]				UID2021 [78]			
	PLCC	SRCC	KRCC	RMSE	PLCC	SRCC	KRCC	RMSE
DIIVINE [33]	0.6487	0.6198	0.4533	16.2230	0.6264	0.6112	0.4363	1.6716
BIQME [39]	0.7470	0.7373	0.5502	14.2362	0.6491	0.6358	0.4566	1.6330
BLIINDS-II [40]	0.4543	0.4264	0.3003	19.0003	0.5451	0.5216	0.3688	1.7934
BRISQUE [41]	0.6066	0.5866	0.4244	16.9051	0.6439	0.6343	0.4623	1.6407
FRIQUEE [42]	0.7888	0.7802	0.5885	13.0257	0.7134	0.7026	0.5035	1.4984
GM-LOG [44]	0.5981	0.5736	0.4096	17.0788	0.5624	0.5384	0.3779	1.7699
GWH-GLBP [45]	0.5011	0.4583	0.3218	18.3530	0.4459	0.4145	0.2875	1.9282
NFERM [46]	0.6520	0.6238	0.4498	16.1554	0.5361	0.5122	0.3608	1.8130
NRSL [47]	0.6421	0.6262	0.4549	16.3618	0.6643	0.6504	0.4655	1.6016
PCRL [48]	0.6530	0.6430	0.4677	16.1583	0.6647	0.6531	0.4725	1.6025
UCIQE [50]	0.5613	0.4992	0.3512	17.5973	0.6474	0.6150	0.4503	1.6335
UIQM [51]	0.4364	0.4061	0.2839	19.2664	0.4760	0.4613	0.3192	1.8769
CCF [52]	0.0995	0.0460	0.0311	21.2575	0.5208	0.4236	0.2990	1.8351
FDUM [53]	0.2949	0.1832	0.1237	20.4524	0.6092	0.5823	0.4189	1.7057
NUIQ [57]	0.7927	0.7914	0.6075	13.0154	0.7266	0.7168	0.5293	1.4762
Proposed	**0.8174**	**0.8164**	**0.6326**	**12.3297**	**0.7423**	**0.7347**	**0.5420**	**1.4404**

We validate the performance of our method on the SAUD dataset [57] and the UID2021 dataset [78].

SAUD Dataset [57]: The SAUD dataset [57] is constructed by gathering 100 authentic underwater images from the UIEB [23] and RUIE [79] datasets as source images, which were then processed using results obtained from 10 distinct state-of-the-art underwater image enhancement algorithms. The authors conducted a subjective user study using the Dual Stimulus Comparison (DSC) method [3], resulting in subjective scores for each image within the SAUD dataset.

UID2021 Dataset [59]: The UID2021 dataset [78] comprises 900 augmented underwater images, which were generated through 60 underwater degraded images using 15 distinct state-of-the-art underwater image enhancement and restoration algorithms. Subjective experiments were conducted on this dataset employing a pairwise comparison ranking method, yielding average opinion scores from 52 observers for each image within the UID2021 dataset.

3.2. Performance Comparisons

The overall performance comparison results are shown in Table 2, and we highlight the best results in bold. From the table, we can see that our proposed method achieves the best prediction performance on the SAUD [57] database and the UID2021 dataset [78], compared to existing NR IQA methods.

Specifically,it outperforms five existing methods for evaluating underwater image quality (i.e., CCF, FDUM, UCIQE, UIQM, NUIQ). Moreover, it surpassed the SRCC value of the second place (i.e., NUIQ) by about 3%.The only reason is that we consider that the color of the underwater image conforms to the characteristics of the Rayleigh distribution, and extract the characteristics of the underwater image from a more comprehensive orientation combined with the characteristics of the color, contrast and visibility of the underwater image.

Secondly, the evaluation methods of underwater images, CCF and FDUM, extract three features of underwater images and weigh each feature as a method for evaluating underwater images. On the SAUD dataset [57], their measured performances are deficient, indicating that the underwater features measured by these two methods are not suitable for underwater images in the SAUD dataset [57]. On the UID2021 dataset [78], the two algorithms, CCF and FDUM, did not perform better than most natural image evaluation algorithms. Through testing on two datasets, we found that the testing method with trained features outperforms the feature weighted method. Evaluation methods that can also reflect trained features in UCIQE and UIQM are more advantageous.

Finally, we test two other methods for underwater image quality assessment (i.e., UCIQE and UIQM), which were developed to evaluate the visual quality of raw underwater images. The SAUD dataset [57] and the UID2021 dataset [78] are collected according to different underwater image enhancement methods.

On the SAUD dataset [57], the SRCC metric of the method proposed in this paper reaches 0.8164, and its percentage gain reaches 38% compared to the UCIQE method, and 50% compared to the UIQM method. On the UID2021 dataset [78], the SRCC metric of the method proposed in this paper reaches 0.7347, and its percentage gain reaches 16% compared to the UCIQE method and 37% compared to the UIQM method. It is obvious that our proposed method has stronger correlation with subjective evaluation on SAUD dataset [57] and UID2021 dataset [78], no matter compared with the existing general-purpose NR-IQA method or underwater IQA.

Table 3: Experimental Results of Cross Dataset Validation. The 'A/B' Means Training on Dataset 'A' and Testing on Dataset 'B'.

Metrics	SAUD/UID2021				UID 2021/SAUD			
	PLCC	SRCC	KRCC	RMSE	PLCC	SRCC	KRCC	RMSE
BIQME [39]	0.2443	0.2525	0.1717	2.0899	0.4323	0.2857	0.1957	19.3102
BLIINDS-II [40]	0.1411	0.1267	0.0843	2.1337	0.1583	0.1258	0.0869	21.2112
BRISQUE [41]	0.2332	0.2173	0.1429	2.0958	0.2818	0.2628	0.1797	20.5467
DIIVINE [33]	0.4327	0.4240	0.2889	1.9430	0.4158	0.3609	0.2490	19.4756
FRIQUEE [42]	0.4311	0.4324	0.2945	1.9447	0.4158	0.3609	0.2490	19.4656
GM-LOG [44]	0.3590	0.3040	0.2066	2.0115	0.4033	0.3561	0.2377	19.5958
GWH-GLBP [45]	0.0407	0.0287	0.0189	2.1534	0.1158	0.1070	0.0715	21.2701
NFERM [46]	0.4764	0.4715	0.3267	1.8949	0.2357	0.1735	0.1140	20.8111
NRSL [47]	0.3620	0.3488	0.2391	2.0091	0.2510	0.2367	0.1623	20.7287
PCRL [48]	0.1866	0.1311	0.0875	2.1174	0.2757	0.2245	0.1529	20.5840
CCF [52]	0.4037	0.3110	0.2146	1.9718	0.4449	0.3597	0.2494	19.1776
FDUM [53]	0.4775	0.4486	0.3061	1.8936	0.2902	0.1655	0.1101	20.4925
UCIQE [50]	0.5032	0.4422	**0.3942**	1.8628	0.4687	0.2448	0.1647	18.9170
UIQM [51]	0.3574	0.3141	0.2122	2.0128	0.3945	0.2368	0.1620	19.6777
NUIQ [57]	0.4351	0.4170	0.2843	1.9434	0.4801	0.4470	0.3127	18.7849
Proposed	**0.5223**	**0.4804**	0.3478	**1.8380**	**0.5644**	**0.5212**	**0.3733**	**17.6775**

In order to test the generalization capability of our method, we conducted cross-dataset experiments on the SAUD dataset [57] and the UID2021 dataset [78]. The results are presented in Table 3 where "SAUD/UID2021" indicates the model is trained on the SAUD dataset [57] and tested on the UID2021 dataset [78], while "UID2021/SAUD" represents the model is trained on the UID2021 dataset [78] and tested on the SAUD dataset [57]. From Table 3, it can be observed that our method performs the best on both cases. This indicates that our approach has superior generalization capability and robustness.

To further verify the proposed method, we utilize a hypothesis test on the basis of t-statistic [80]. In our experiments, a two-sample t-test was performed on a pair of SRCC values for 1,000 training trials at the 5% significance level. Fig. 12 shows the results of the t-test, where a value of 1/-1 indicates that the row metric is statistically better/worse than the column metric, and a value of 0 indicates that the row metric is statistically competitive with the column metric. From the results shown in this figure, we observe that the performance of the proposed method is better than that of all competing methods, which further

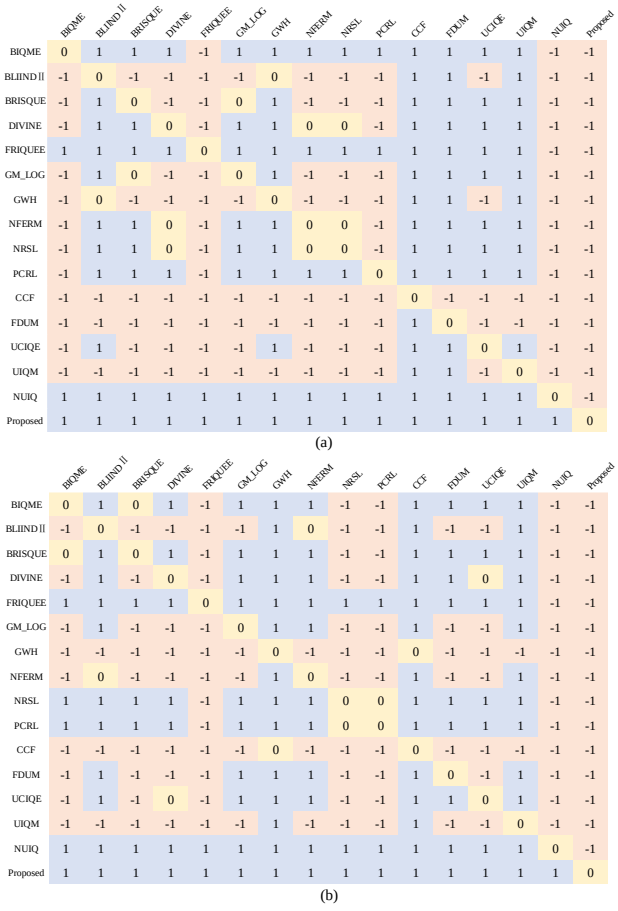

Figure 12: Two-sample t-test results between the pair of SROCC values of 1,000 train-test trails at the 5% significance level. (a) SAUD, (b) UID2021.

illustrates the superiority of our method.

3.3. Parameter Tests

Since the performance of learning-based methods are sensitive to the partition of training-testing subsets, we adjust the percentages of training sets to verify the performance of our model. Therefore, we increase the training set from 20% to 80% with an interval of 10%, and the results are shown in Table 4. It can be seen that as the proportion of the training set increases, the values of SRCC, KRCC, and PLCC increase, and the RMSE value decreases. That is, the performance of the proposed method

Table 4: Performance Under Varying Train-Test Splits On SAUD dataset and UID2021 dataset.

Train-Test Split	SAUD [57]				UID2021 [78]			
	PLCC	SRCC	KRCC	RMSE	PLCC	SRCC	KRCC	RMSE
20%-80%	0.6808	0.6803	0.4984	15.6563	0.5797	0.5742	0.4068	1.7526
30%-70%	0.7260	0.7264	0.5400	14.7086	0.6033	0.5990	0.4262	1.7140
40%-60%	0.7535	0.7533	0.5662	14.0443	0.6133	0.6089	0.4346	1.6995
50%-50%	0.7768	0.7769	0.5895	13.4698	0.6744	0.6710	0.4859	1.5870
60%-40%	0.7937	0.7935	0.6061	13.0282	0.6816	0.6779	0.4918	1.5704
70%-30%	0.7998	0.8006	0.6153	12.8265	0.7186	0.7148	0.5253	1.4917
80%-20%	0.8174	0.8164	0.6326	12.3297	0.7423	0.7347	0.5420	1.4404

proposed improves accordingly with the increased percentage of training subset. Moreover, when our training subset only occupies 40% of all samples, our method still outperforms most other existing methods, which further demonstrates the superiority and stability of our proposed method.

Furthermore, since our method is composed of multiple image attributes, exploring the effects of different features and their combinations on the final performance is interesting. Here, we first conduct experiments with the features extracted from each attribute by fedding the features from each attribute into the SVR to learn the prediction model, and evaluate the performance through the same four criteria (i.e., SRCC, KRCC, PLCC, RMSE). Second, the attributes of our method are combined in pairs, and the same operation as the previous step is performed. Finally, the three attributes are combined in the experiment. The comparison results are shown in Table 5, where the symbol "✔" ("✘") denotes that the feature in the column is included (not included) in our framework. For the observation convenience, we adopt C_c, C_t, and V_s to represent the features extracted in the aspects of color, contrast, and visibility.

3.4. Computational Complexity

A good quality assessment method for underwater images should be both accurate and fast. Thus, we compare our model with other competing methods in terms of running time. Specifically, we set up a running time comparison of different competing methods and show the corresponding SRCC values to better illustrate the relationship between equilibration time and effect, as shown in Fig. 13. We can see that the proposed method achieves the best SRCC value at a moderate time complexity. This is

Table 5: Result Under Different Attribute Combinations.

Model	C_c	C_t	V_s	PLCC	SRCC	KRCC	RMSE
Model_1	✔	✘	✘	0.7163	0.7116	0.5311	14.8741
Model_2	✘	✔	✘	0.7443	0.7614	0.5764	13.6996
Model_3	✘	✘	✔	0.4359	0.3645	0.2512	19.1621
Model_4	✔	✔	✘	0.7676	0.7969	0.6113	12.8493
Model_5	✔	✘	✔	0.7484	0.7397	0.5556	14.1059
Model_6	✘	✔	✔	0.7780	0.7727	0.5867	13.3543
Proposed	✔	✔	✔	0.8174	0.8164	0.6326	12.3297

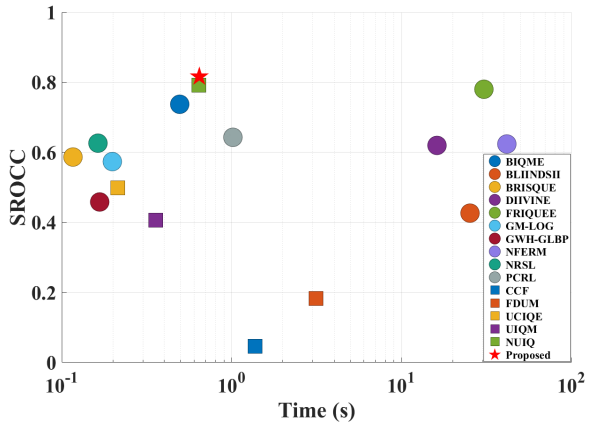

Figure 13: Comparison of different NR IQA metrics in terms of the running time and SROCC value.

promising in practical applications regarding the balance of computational time and accuracy.

3.5. Model Comparison

We conducted experiments using various regression models, and the experimental results are presented in Table 6. For the SAUD dataset, we selected different regression models, and the results indicate that the SVR model outperforms the others. The primary reasons for its superior performance include its capability to handle nonlinear data and noise, control overfitting, effectiveness in dealing with high-dimensional data, flexibility, global optimization, and applicability in outlier detection. In our study, we extracted three feature sets, and these feature sets exhibit no linear relationships among them, resulting in a total of 42-dimensional features. Given the high feature dimensionality, SVR is considered the most suitable regression model based on the characteristics of these features. The results also demonstrate the effectiveness of SVR.

Table 6: Model Performance Comparison on the SAUD Dataset.

Model	PLCC	SRCC	KRCC	RMSE
Decision Tree	0.6096	0.5957	0.4407	18.2379
Random Forest	0.6976	0.6923	0.5153	16.0354
Bayesian Regression	0.7352	0.7328	0.5374	13.5429
SVR	0.8174	0.8164	0.6326	12.3297

4. Conclusion

In this paper, we propose a new no-reference quality assessment method for underwater image enhancement. Specifically, we consider three kinds of quality-sensitive features, including colorfulness, contrast, and visibility. After the feature extraction, we map the extracted features into the corresponding quality scores by a regression model. Experimental results show that the proposed method outperforms state-of-the-art NR IQA methods in evaluating underwater image quality. To date, only a very limited number of underwater image databases have been established, thereby constraining the progress within the field of underwater image quality assessment. In future research endeavors, we will focus on the development of a large-scale underwater image database, which will constitute one of our primary objectives for future investigations. Furthermore, traditional objective image quality assessment methods fail to guarantee the accuracy of objective prediction scores, as these conventional approaches inherently possess a degree of subjectivity. In future research, we will explore quality assessment methodologies rooted in deep learning and more advanced learning pipelines [81], capable of autonomously learning discriminative features of degraded underwater images, with the potential to promote the advancement of underwater image enhancement algorithms.

Acknowledgments

This work was supported in part by the Natural Science Foundation of China (62271277), in part by the Natural Science Foundation of Zhejiang (LR22F020002), and in part by the Natural Science Foundation of Ningbo (2022J081).

References

[1] Y. Y. Schechner, N. Karpel, Recovery of underwater visibility and structure by polarization analysis, IEEE Journal of oceanic engineering 30 (3) (2005) 570–587.

[2] Z. Li, J. Zheng, Edge-preserving decomposition-based single image haze removal, IEEE Transactions on Image Processing 24 (12) (2015) 5432–5441.

[3] J. Han, K. Yang, M. Xia, L. Sun, Z. Cheng, H. Liu, J. Ye, Resolution enhancement in active underwater polarization imaging with modulation transfer function analysis, Applied Optics 54 (11) (2015) 3294–3302.

[4] X. Zhao, T. Jin, S. Qu, Deriving inherent optical properties from background color and underwater image enhancement, Ocean Engineering 94 (2015) 163–172.

[5] H. Lu, Y. Li, X. Xu, J. Li, Z. Liu, X. Li, J. Yang, S. Serikawa, Underwater image enhancement method using weighted guided trigonometric filtering and artificial light correction, Journal of Visual Communication and Image Representation 38 (2016) 504–516.

[6] G. N. Bailey, N. C. Flemming, Archaeology of the continental shelf: marine resources, submerged landscapes and underwater archaeology, Quaternary Science Reviews 27 (23-24) (2008) 2153–2165.

[7] J. Cheng, Z. Wu, S. Wang, C. Demonceaux, Q. Jiang, Bidirectional collaborative mentoring network for marine organism detection and beyond, IEEE Transactions on Circuits and Systems for Video Technology 33 (11) (2023) 6595–6608.

[8] J. Hu, Q. Jiang, R. Cong, W. Gao, F. Shao, Two-branch deep neural network for underwater image enhancement in hsv color space, IEEE Signal Processing Letters 28 (2021) 2152–2156.

[9] L. Chen, Z. Jiang, L. Tong, Z. Liu, A. Zhao, Q. Zhang, J. Dong, H. Zhou, Perceptual underwater image enhancement with deep learning and physical priors, IEEE Transactions on Circuits and Systems for Video Technology 31 (8) (2020) 3078–3092.

[10] X. Ye, Z. Li, B. Sun, Z. Wang, R. Xu, H. Li, X. Fan, Deep joint depth estimation and color correction from monocular underwater images based on unsupervised adaptation networks, IEEE Transactions on Circuits and Systems for Video Technology 30 (11) (2019) 3995–4008.

[11] Y. Zhou, Q. Wu, K. Yan, L. Feng, W. Xiang, Underwater image restoration using color-line model, IEEE Transactions on Circuits and Systems for Video Technology 29 (3) (2018) 907–911.

[12] Q. Qi, Y. Zhang, F. Tian, Q. J. Wu, K. Li, X. Luan, D. Song, Underwater image co-enhancement with correlation feature matching and joint learning, IEEE Transactions on Circuits and Systems for Video Technology 32 (3) (2021) 1133–1147.

[13] W. Song, Y. Wang, D. Huang, A. Liotta, C. Perra, Enhancement of underwater images with statistical model of background light and optimization of transmission map, IEEE Transactions on Broadcasting 66 (1) (2020) 153–169.

[14] C.-Y. Li, J.-C. Guo, R.-M. Cong, Y.-W. Pang, B. Wang, Underwater image enhancement by dehazing with minimum information loss and histogram distribution prior, IEEE Transactions on Image Processing 25 (12) (2016) 5664–5677.

[15] A. S. Abdul Ghani, N. A. Mat Isa, Underwater image quality enhancement through composition of dual-intensity images and rayleigh-stretching, SpringerPlus 3 (1) (2014) 1–14.

[16] X. Fu, P. Zhuang, Y. Huang, Y. Liao, X.-P. Zhang, X. Ding, A retinex-based enhancing approach for

single underwater image, in: 2014 IEEE international conference on image processing (ICIP), IEEE, 2014, pp. 4572–4576.

[17] D. Huang, Y. Wang, W. Song, J. Sequeira, S. Mavromatis, Shallow-water image enhancement using relative global histogram stretching based on adaptive parameter acquisition, in: International conference on multimedia modeling, Springer, 2018, pp. 453–465.

[18] X. Fu, Z. Fan, M. Ling, Y. Huang, X. Ding, Two-step approach for single underwater image enhancement, in: 2017 international symposium on intelligent signal processing and communication systems (ISPACS), IEEE, 2017, pp. 789–794.

[19] Y. Kang, Q. Jiang, C. Li, W. Ren, H. Liu, P. Wang, A perception-aware decomposition and fusion framework for underwater image enhancement, IEEE Transactions on Circuits and Systems for Video Technology 33 (3) (2023) 988–1002.

[20] P. L. Drews, E. R. Nascimento, S. S. Botelho, M. F. M. Campos, Underwater depth estimation and image restoration based on single images, IEEE computer graphics and applications 36 (2) (2016) 24–35.

[21] C. Li, S. Anwar, F. Porikli, Underwater scene prior inspired deep underwater image and video enhancement, Pattern Recognition 98 (2020) 107038.

[22] X. Fu, X. Cao, Underwater image enhancement with global–local networks and compressed-histogram equalization, Signal Processing: Image Communication 86 (2020) 115892.

[23] C. Li, C. Guo, W. Ren, R. Cong, J. Hou, S. Kwong, D. Tao, An underwater image enhancement benchmark dataset and beyond, IEEE Transactions on Image Processing 29 (2019) 4376–4389.

[24] P. Zhu, Y. Liu, Y. Wen, M. Xu, X. Fu, S. Liu, Unsupervised underwater image enhancement via content-style representation disentanglement, Engineering Applications of Artificial Intelligence 126 (2023) 106866.

[25] J. Zhou, Q. Liu, Q. Jiang, W. Ren, K. M. Lam, W. shi Zhang, Underwater camera: Improving visual perception via adaptive dark pixel prior and color correction, International Journal of Computer Vision (2023).

[26] Q. Jiang, Y. Mao, R. Cong, W. Ren, C. Huang, F. Shao, Unsupervised decomposition and correction network for low-light image enhancement, IEEE Transactions on Intelligent Transportation Systems 23 (10) (2022) 19440–19455.

[27] Z. Wang, A. C. Bovik, Mean squared error: Love it or leave it? a new look at signal fidelity measures, IEEE signal processing magazine 26 (1) (2009) 98–117.

[28] Z. Wang, A. C. Bovik, H. R. Sheikh, E. P. Simoncelli, Image quality assessment: from error visibility to structural similarity, IEEE transactions on image processing 13 (4) (2004) 600–612.

[29] H. Hadizadeh, I. V. Bajić, Full-reference objective quality assessment of tone-mapped images, IEEE Transactions on Multimedia 20 (2) (2017) 392–404.

[30] J. Xu, W. Zhou, H. Li, F. Li, Q. Jiang, Quality assessment of multi-exposure image fusion by synthesizing local and global intermediate references, Displays 74 (2022) 102188.

[31] Z. Wan, K. Gu, D. Zhao, Reduced reference stereoscopic image quality assessment using sparse representation and natural scene statistics, IEEE Transactions on Multimedia 22 (8) (2019) 2024–2037.

[32] W. Chen, K. Gu, T. Zhao, G. Jiang, P. Le Callet, Semi-reference sonar image quality assessment based on task and visual perception, IEEE Transactions on Multimedia 23 (2020) 1008–1020.

[33] A. K. Moorthy, A. C. Bovik, Blind image quality assessment: From natural scene statistics to perceptual quality, IEEE transactions on Image Processing 20 (12) (2011) 3350–3364.

[34] A. Mittal, R. Soundararajan, A. C. Bovik, Making a “completely blind” image quality analyzer, IEEE Signal processing letters 20 (3) (2012) 209–212.

[35] A. Mittal, A. K. Moorthy, A. C. Bovik, Blind/referenceless image spatial quality evaluator, in: 2011 conference record of the forty fifth asilomar conference on signals, systems and computers (ASILOMAR), IEEE, 2011, pp. 723–727.

[36] K. Gu, S. Wang, G. Zhai, S. Ma, X. Yang, W. Lin, W. Zhang, W. Gao, Blind quality assessment of tone-mapped images via analysis of information, naturalness, and structure, IEEE Transactions on Multimedia 18 (3) (2016) 432–443.

[37] L. Li, W. Xia, W. Lin, Y. Fang, S. Wang, No-reference and robust image sharpness evaluation based on multiscale spatial and spectral features, IEEE Transactions on Multimedia 19 (5) (2016) 1030–1040.

[38] Y. Liu, K. Gu, S. Wang, D. Zhao, W. Gao, Blind quality assessment of camera images based on low-level and high-level statistical features, IEEE Transactions on Multimedia 21 (1) (2018) 135–146.

[39] K. Gu, D. Tao, J.-F. Qiao, W. Lin, Learning a no-reference quality assessment model of enhanced images with big data, IEEE transactions on neural networks and learning systems 29 (4) (2017) 1301–1313.

[40] M. A. Saad, A. C. Bovik, C. Charrier, Blind image quality assessment: A natural scene statistics approach in the dct domain, IEEE transactions on Image Processing 21 (8) (2012) 3339–3352.

[41] A. Mittal, A. K. Moorthy, A. C. Bovik, No-reference image quality assessment in the spatial domain, IEEE Transactions on image processing 21 (12) (2012) 4695–4708.

[42] D. Ghadiyaram, A. C. Bovik, Perceptual quality prediction on authentically distorted images using a bag of features approach, Journal of vision 17 (1) (2017) 32–32.

[43] Q. Jiang, Z. Liu, K. Gu, F. Shao, X. Zhang, H. Liu, W. Lin, Single image super-resolution quality assessment: A real-world dataset, subjective studies, and an objective metric, IEEE Transactions on Image Processing 31 (2022) 2279–2294.

[44] W. Xue, X. Mou, L. Zhang, A. C. Bovik, X. Feng, Blind image quality assessment using joint statistics of gradient magnitude and laplacian features, IEEE Transactions on Image Processing 23 (11) (2014) 4850–4862.

[45] Q. Li, W. Lin, Y. Fang, No-reference quality assessment for multiply-distorted images in gradient domain, IEEE Signal Processing Letters 23 (4) (2016) 541–545.

[46] K. Gu, G. Zhai, X. Yang, W. Zhang, Using free energy principle for blind image quality assessment, IEEE Transactions on Multimedia 17 (1) (2014) 50–63.

[47] Q. Li, W. Lin, J. Xu, Y. Fang, Blind image quality assessment using statistical structural and luminance features, IEEE Transactions on Multimedia 18 (12) (2016) 2457–2469.

[48] B. Hu, L. Li, H. Liu, W. Lin, J. Qian, Pairwise-comparison-based rank learning for benchmarking image restoration algorithms, IEEE Transactions on Multimedia 21 (8) (2019) 2042–2056.

[49] Q. Jiang, Z. Peng, G. Yue, H. Li, F. Shao, No-reference image contrast evaluation by generating bidirectional pseudoreferences, IEEE Transactions on Industrial Informatics 17 (9) (2021) 6062–6072.

[50] M. Yang, A. Sowmya, An underwater color image quality evaluation metric, IEEE Transactions on Image Processing 24 (12) (2015) 6062–6071.

[51] K. Panetta, C. Gao, S. Agaian, Human-visual-system-inspired underwater image quality measures, IEEE Journal of Oceanic Engineering 41 (3) (2015) 541–551.

[52] Y. Wang, N. Li, Z. Li, Z. Gu, H. Zheng, B. Zheng, M. Sun, An imaging-inspired no-reference underwater color image quality assessment metric, Computers & Electrical Engineering 70 (2018) 904–913.

[53] N. Yang, Q. Zhong, K. Li, R. Cong, Y. Zhao, S. Kwong, A reference-free underwater image quality assessment metric in frequency domain, Signal Processing: Image Communication 94 (2021) 116218.

[54] H. Lin, H. Men, Y. Yan, J. Ren, D. Saupe, Crowdsourced quality assessment of enhanced underwater images-a pilot study, in: 2022 14th International Conference on Quality of Multimedia Experience (QoMEX), IEEE, 2022, pp. 1–4.

[55] Y. Zheng, W. Chen, R. Lin, T. Zhao, P. Le Callet, Uif: An objective quality assessment for underwater image enhancement, IEEE Transactions on Image Processing 31 (2022) 5456–5468.

[56] P. Guo, H. Liu, D. Zeng, T. Xiang, L. Li, K. Gu, An underwater image quality assessment metric, IEEE Transactions on Multimedia (2022).

[57] Q. Jiang, Y. Gu, C. Li, R. Cong, F. Shao, Underwater image enhancement quality evaluation: Benchmark dataset and objective metric, IEEE Transactions on Circuits and Systems for Video Technology (2022).

[58] P. Guo, L. He, S. Liu, D. Zeng, H. Liu, Underwater image quality assessment: Subjective and objective methods, IEEE Transactions on Multimedia 24 (2021) 1980–1989.

[59] Y. Liu, K. Gu, J. Cao, S. Wang, G. Zhai, J. Dong, S. Kwong, Uiqi: A comprehensive quality evaluation index for underwater images, IEEE Transactions on Multimedia (2023).

[60] Z. Wang, L. Shen, Z. Wang, Y. Lin, Y. Jin, Generation-based joint luminance-chrominance learning for underwater image quality assessment, IEEE Transactions on Circuits and Systems for Video Technology 33 (3) (2022) 1123–1139.

[61] Y. Kang, Q. Jiang, C. Li, W. Ren, H. Liu, P. Wang, A perception-aware decomposition and fusion framework for underwater image enhancement, IEEE Transactions on Circuits and Systems for Video Technology (2022).

[62] S.-B. Gao, K.-F. Yang, C.-Y. Li, Y.-J. Li, Color constancy using double-opponency, IEEE transactions on pattern analysis and machine intelligence 37 (10) (2015) 1973–1985.

[63] L. K. Choi, J. You, A. C. Bovik, Referenceless prediction of perceptual fog density and perceptual image defogging, IEEE Transactions on Image Processing 24 (11) (2015) 3888–3901.

[64] X.-S. Zhang, S.-B. Gao, R.-X. Li, X.-Y. Du, C.-Y. Li, Y.-J. Li, A retinal mechanism inspired color constancy model, IEEE Transactions on Image Processing 25 (3) (2016) 1219–1232.

[65] S. Gao, K. Yang, C. Li, Y. Li, A color constancy model with double-opponency mechanisms, in: Proceedings of the IEEE international conference on computer vision, 2013, pp. 929–936.

[66] D. Hasler, S. E. Suesstrunk, Measuring colorfulness in natural images, in: Human vision and electronic imaging VIII, Vol. 5007, SPIE, 2003, pp. 87–95.

[67] B. McGlamery, A computer model for underwater camera systems, in: Ocean Optics VI, Vol. 208, SPIE, 1980, pp. 221–231.

[68] D. Akkaynak, T. Treibitz, A revised underwater image formation model, in: Proceedings of the IEEE conference on computer vision and pattern recognition, 2018, pp. 6723–6732.

[69] Y. Fang, K. Ma, Z. Wang, W. Lin, Z. Fang, G. Zhai, No-reference quality assessment of contrast-distorted images based on natural scene statistics, IEEE Signal Processing Letters 22 (7) (2014) 838–842.

[70] N. V. S. Graham, Visual pattern analyzers, Oxford University Press, 1989.

[71] J. S. Jaffe, Computer modeling and the design of optimal underwater imaging systems, IEEE Journal of Oceanic Engineering 15 (2) (1990) 101–111.

[72] J. Jaffe, Underwater optical imaging: the past, the present, and the prospects, IEEE Journal of Oceanic Engineering 40 (3) (2014) 683–700.

[73] Y. Liu, K. Gu, G. Zhai, X. Liu, D. Zhao, W. Gao, Quality assessment for real out-of-focus blurred images, Journal of Visual Communication and Image Representation 46 (2017) 70–80.

[74] R. Ferzli, L. J. Karam, A no-reference objective image sharpness metric based on the notion of just noticeable blur (jnb), IEEE transactions on image processing 18 (4) (2009) 717–728.

[75] P. V. Vu, D. M. Chandler, A fast wavelet-based algorithm for global and local image sharpness estimation, IEEE Signal Processing Letters 19 (7) (2012) 423–426.

[76] A. Cohen, I. Daubechies, J.-C. Feauveau, Biorthogonal bases of compactly supported wavelets, Communications on pure and applied mathematics 45 (5) (1992) 485–560.

[77] C. J. Burges, A tutorial on support vector machines for pattern recognition, Data mining and knowledge discovery 2 (2) (1998) 121–167.

[78] G. Hou, Y. Li, H. Yang, K. Li, Z. Pan, Uid2021: An underwater image dataset for evaluation of no-reference quality assessment metrics, ACM Transactions on Multimedia Computing, Communications and Applications 19 (4) (2023) 1–24.

[79] R. Liu, X. Fan, M. Zhu, M. Hou, Z. Luo, Real-world underwater enhancement: Challenges, benchmarks, and solutions under natural light, IEEE transactions on circuits and systems for video technology 30 (12) (2020) 4861–4875.

[80] D. C. Montgomery, G. C. Runger, Applied statistics and probability for engineers, John wiley & sons, 2010.

[81] H. Wang, M. Yao, G. Jiang, Z. Mi, X. Fu, Graph-collaborated auto-encoder hashing for multiview binary clustering, IEEE Transactions on Neural Networks and Learning Systems (2023).